



Nitrogen-doped hollow carbon spheres for electrochemical detection of heavy metal ions

Mei Liu¹ · Qing Guan¹ · Shantang Liu¹

Received: 1 March 2017 / Revised: 10 November 2017 / Accepted: 6 December 2017 / Published online: 15 December 2017
© Springer-Verlag GmbH Germany, part of Springer Nature 2017

Abstract

Nitrogen-doped hollow carbon spheres (N-HCSs) were successfully fabricated using silica sphere as template and resorcinol-formaldehyde resin as carbon precursor. Scanning electron microscopy and transmission electron microscopy demonstrated that diameters and shell thickness of N-HCSs were 325 and 25 nm, respectively. The N-HCS modified gold electrode was used for the square wave anodic stripping voltammetry for the individual determination of trace heavy metal ions (HMIs) such as Pb^{2+} , Cu^{2+} , and Hg^{2+} in drinking water. Electrochemical properties of modified electrode were characterized by cyclic voltammetry and electrochemical impedance spectroscopy. Moreover, the supporting electrolytes, pH, deposition potential, and deposition time were carefully studied. The N-HCS modified electrode exhibited the detection limit of 15, 17, and 2.35 nM for Pb^{2+} , Cu^{2+} , and Hg^{2+} , respectively, which are significantly lower than the guideline values for drinking water quality provided by the World Health Organization. The electrochemical measurement results showed that the N-HCS structures exhibited wonderful adsorption and capacitive properties toward HMIs and were found to be useful for the simultaneous and selective electrochemical detection. Most importantly, herein we discussed the two types of test for simultaneous detection of Pb^{2+} and Hg^{2+} , under the optimum experimental conditions. The sensitivity of Hg^{2+} increased in the presence of concentration range of Pb^{2+} . Thus, this study provides a reliable method for online detection of low concentration Hg^{2+} and robust alternatives for heavy metal sensors.

Keywords Nitrogen doped · Hollow carbon sphere · Electrochemical · Heavy metal ions

Introduction

Toxic heavy metal ions (HMIs) are well known to be extremely harmful to environment and human health [1]. Therefore, the development of rapid and sensitive methods for their detection and monitoring has attracted significant attention in recent years [2, 3]. Numerous mature approaches, such as flame atomic absorption spectrometry, atomic fluorescence spectrometry, spectrophotometry, cathodic adsorptive stripping voltammetry, anodic stripping voltammetry, and electrochemical impedance spectroscopy (EIS), have been employed so far for detection of heavy metals [4–8]. In these developed approaches, electrochemical analysis, in particular, the anodic

stripping voltammetry method as a powerful technique provides a promising and elegant tool for the effective detection of metal ions. This method possesses high sensitivity and can simultaneously analyze several HMIs [9–13]. Electrode materials are the main contributors to the electrochemical detection of the HMIs. Among various modified electrode materials, carbon-based electrode materials have become very popular alternatives in recent years due to their low cost, remarkable conductivities, broad potential range, and portable modification [14, 15]. Among various carbon-based electrode materials, porous carbon materials with a large surface area and graphitic structure offer great advantages in electrocatalysis and electrochemical detections. For these reason, hollow carbon nanospheres (HCSs) have been applied in many fields because of their low density, shell permeability, good electrical conductivity, and chemical stability [8]. For example, Liu's group prepared highly ordered three-dimensional macroporous carbon sphere modified electrode, which exhibited excellent electrochemical response of carbon materials for detection of HMIs [12]. Moreover, their high surface-to-volume ratio, integrating of hollow inner space, and stable

✉ Shantang Liu
stliu@wit.edu.cn

¹ Key Laboratory for Green Chemical Process of Ministry of Education, School of Chemistry and Environmental Engineering, Wuhan Institute of Technology, Wuhan 430074, People's Republic of China

structural significantly enhance the performances of electrochemical determination of HMIs [16, 17].

Many studies have reported that hollow carbon structures can be applied in catalysis, water treatment, lithium-ion battery, and supercapacitors [18–21]. However, to the best of our knowledge, the application of HCSs in electrochemical sensors has rarely been investigated. The unique properties enable HCSs to have certain potential applications favoring the development of highly sensitive electrochemical sensors. Besides, most recently, it has been reported that nitrogen doping could play an important role in regulating the electronic properties and enhancing the electrocatalytic activity of carbon materials [22–26]. In particular, it has been demonstrated that functionalizing carbon nanomaterials with nitrogen groups can significantly boost their applications because they lead to the enhancement in their electronic conductivity, surface polarity, surface basic sites, and surface wettability of the carbon matrix [19, 27–31]. Thus, these advantages convinced us that the use of nitrogen-doped HCSs (N-HCSs) for electrochemical sensing is of great significance.

In this study, hollow-structured carbon spheres were fabricated using resorcinol formaldehyde as carbon precursor and tetraethyl orthosilicate (TEOS) as a structure-assistant agent, in a mixture containing water, ethanol, and ammonia. Carbonization was followed by etching of the silica in the carbon/silica nanocomposite. Doping with heteroatoms such as nitrogen seems to be an exciting approach for introducing original function atoms to carbonaceous materials including extraordinary electronic properties and enhanced reactivity with increased defect sites to anchor guest molecules [32–34]. The remarkable properties make it a significantly potential candidate as electrode materials for HMI sensing. Square wave anodic stripping voltammetry (SWASV) with its excellent sensitivity was used for the detection of HMIs. The N-HCS modified gold electrode showed an excellent sensitivity, selectivity, and stability for the analysis of Hg^{2+} , Cu^{2+} , and Pb^{2+} due to their hollow interior and N-doped thin shell. Thus, this research focused on the application of nitrogen-doped carbonaceous materials for electrochemical sensing of HMIs, and carbon-nitrogen modified electrode was explored successfully for the desired purpose.

Experiment section

Chemicals and reagents

HCHO, $\text{C}_3\text{N}_3(\text{NH}_2)_3$, $\text{C}_6\text{H}_4(\text{OH})_2$, $\text{Si}(\text{OC}_2\text{H}_5)_4$, $\text{C}_{16}\text{H}_{33}(\text{CH}_3)_3\text{NBr}$, $\text{NH}_3\cdot\text{H}_2\text{O}$, NaOH, $\text{K}_3\text{Fe}(\text{CN})_6$, $\text{K}_4\text{Fe}(\text{CN})_6$, $\text{Pb}(\text{NO}_3)_2$, $\text{CuSO}_4\cdot 5\text{H}_2\text{O}$, HAc, and NaAc reagents were purchased from Sinopharm Chemical Reagent Ltd. Stock solutions of $\text{Pb}(\text{NO}_3)_2$ and CuSO_4 (0.01 mol/L) were prepared by directly dissolving $\text{Pb}(\text{NO}_3)_2$ and CuSO_4

$5\text{H}_2\text{O}$, respectively, in deionized water. All reagents were of analytical grade, and doubly distilled water was used throughout the experiments.

Apparatus

Fourier transform infrared spectrometry (FT-IR) measurements were performed on a Nicolet 750 (America). Scanning electron microscope (SEM) images and energy dispersive X-ray spectroscopy (EDS) were performed by JSM-5510LV micro-scope (Japan). X-ray photoelectron spectra (XPS) were recorded by a K-Alpha spectrometer (Thermo Fisher Scientific Inc., Switzerland) equipped with a monochromatic Al $\text{K}\alpha$ source operated at 150 W. Electrochemical measurements were carried out on CHI 660C electrochemical workstation (Shanghai, China). The conventional three-electrode system involved modified electrodes as working electrode, a platinum wire as auxiliary electrode, and a saturated calomel as reference electrode (SCE).

Synthesis of N-HCSs

Typically, ammonia aqueous solution (NH_4OH , 25 wt%, 3 mL) was mixed with a solution containing absolute ethanol (EtOH, 75 mL), deionized water (H_2O , 10 mL), and CTAB (0.5 g) at 70 °C under vigorous stirring for 30 min. After that, resorcinol (0.55 g) was added then continually stirred for 30 min. Then TEOS (3 mL) and formaldehyde solution (0.74 mL) were added to the reaction solution and stirred for another 30 min until a complete dissolution occurred. In a typical coating process, the as-prepared SiO_2 colloidal solution was sequentially combined with CTAB (3 mL, 0.01 M), vigorously stirred for 30 min to ensure the complete adsorption of CTAB on the silica surface. Next, 0.55 mL of formaldehyde and 0.3 g melamine was added to the above mixture and stirred for 12 h at 70 °C. The solid product was recovered by centrifugation and air-dried at 70 °C overnight. Calcination was carried out in a tubular furnace at 600 °C for 2 h under N_2 flow with the heating rate of 3 °C min^{-1} . After removing the silica component by etching in NaOH solution (1 M), N-HCSs were obtained. The synthesis method is illustrated in Scheme 1.

Fabrication of the N-HCS modified electrode

Prior to modification, bare GCE (diameter 2 mm) was carefully polished with 0.05 μm alumina slurry until a mirror shine surface was obtained, followed by successively sonicating in doubly deionized water, absolute ethanol, and doubly deionized water for 5 min, respectively. The N-HCS was bound to the electrode surface using chitosan (Chit) as a binder. N-HCS (50 mg) was dispersed in 1 mg/mL chit solution (10 ml) with the aid of ultrasonic agitation. The N-HCS modified electrode was obtained by pipetting 6 μL of the mixture to the surface of the gold electrode,

Scheme 1 Schematic depiction of the synthesis of N-HCS



followed by drying in air at room temperature. The modified electrode surface was found to be hydrophilic.

Hg²⁺, Pb²⁺, and Cu²⁺ detection

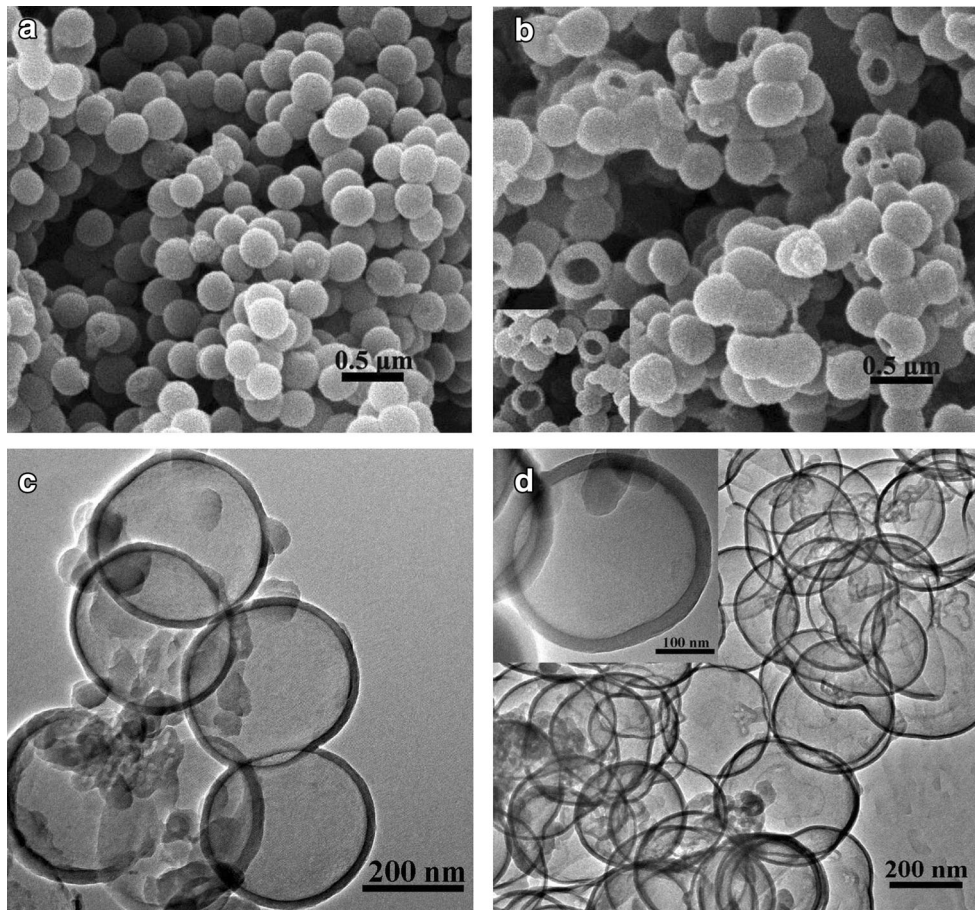
SWASV was used for the detection under optimized conditions. All measurements were carried out in 0.1 M NaAc-HAc buffer solution (pH 5.0) containing the target metals ions and the target metals ions were deposited on the surface of N-HCS/CS modified electrode by holding potential of -1.2 V for 150 s in a stirred solution. After standing for 15 s, the SWASV measurements were performed under the following conditions: a frequency of 15 Hz; amplitude of 25 mV; pulse

width of 50 ms; and potential step of 4 mV. The simultaneous and selective detection of Hg²⁺ and Pb²⁺ has been performed at the same experimental condition.

Result and discussion

The polymer spheres were fabricated by polymerization of resorcinol/formaldehyde/melamine and TEOS in a mixture of ethanol, cetyltrimethylammonium bromide (CTAB), and ammonia. The morphology and microstructure of the prepared samples were characterized by the scanning electron microscopy (SEM). Figure 1a exhibits uniform spherical

Fig. 1 a SEM image of SiO₂, b SEM image of N-HCS, c and d TEM image of typical sample N-HCS



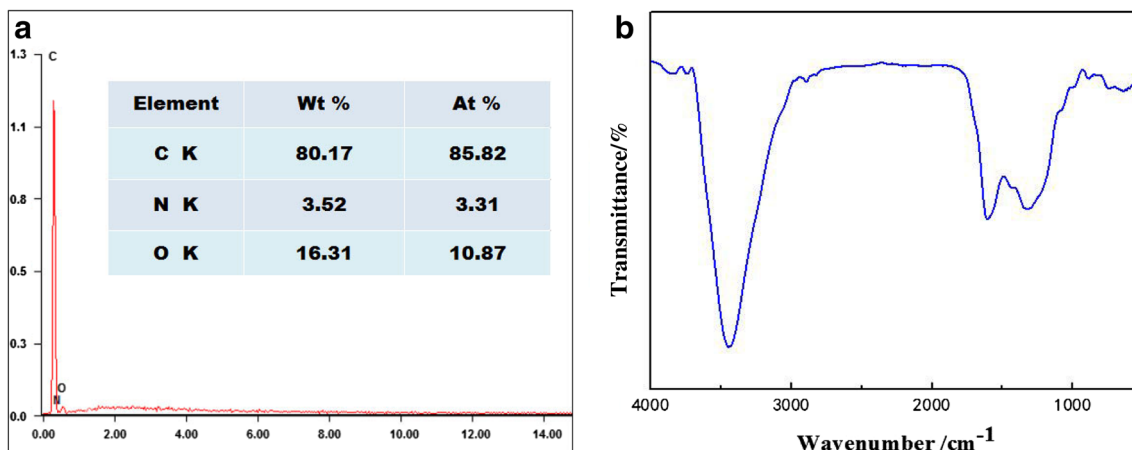


Fig. 2 XPS of N-HCSs sample **a** survey, **b** N1s

morphology of the silica sub-microsphere with particle average diameter of approximately 300 nm. After carbonization and etching of the template, all the N-HCS samples mainly inherited the spherical structure with a rough surface. Figure 1b clearly demonstrates some broken sub-microsphere with apparent cavities, indicating the hollow structure of the sub-microsphere. The transmission electron microscopy (TEM) images of HCS displayed in Fig. 1c and d further showed that the sub-microsphere present as lighter contrast in the center, indicating the hollow structure with cavity size of about 325 nm. The darker rims corresponded to the shells of the sub-microsphere, which exhibited the wall thickness of these spheres was around 25 nm.

Figure 2 shows the results of energy-dispersive X-ray spectroscopy (EDS) mapping and Fourier transform infrared (FTIR) spectroscopy performed on hollow sub-microsphere. Figure 2a exhibits the distribution of C and N in the shell of N-HCSs, the elemental peak of N appears corresponding to the sample, and its content in hollow N-doped carbon sub-microsphere was detected to be 3.31 wt% by using an elemental analyzer. The peak at 1350 and 1601.9 cm^{-1} correspond to C–N bonds and peak at 3491.2 cm^{-1} can be attributed to the stretching vibration of the N–H bond. These results indicate the successful fabrication of a hierarchical nanostructured N-HCSs by the proposed method.

The XPS spectra are employed to investigate the surface composition and the chemical state of the N-HCSs. Figure 3 shows three typical peaks for C1s, O1s, and N1s on wide XPS survey spectrum with the corresponding content of each element of 90.32, 6.57, and 3.11 wt%, and the elemental compositions of N-HCSs are present in Table 1. This is consistent with results from earlier EDX results. The result suggested that nitrogen elements have been retained on the carbon frameworks in carbonization process. In general, the nitrogen-doping is beneficial to the conductivity and electron transfer of carbon materials [28]. Meanwhile, its electrical property would change, because the nitrogen has one more

valence electron than carbon resulting in new energy levels which can lower the conduction band [29].

Cyclic voltammetry and electrochemical impedance spectroscopy characterization of N-HCSs

Figure 4a displays the cyclic voltammogram (CV) responses of bare gold electrode and N-HCSs/CS modified gold electrode in 5 mM $\text{Fe}(\text{CN})_6^{3-/4-}$ containing 0.1 M KCl. The current response of HCSs/CS and N-HCSs/CS toward $\text{Fe}(\text{CN})_6^{3-/4-}$ was larger than that of the bare electrode, suggesting that the electrochemical active sites of gold electrode was increased by HCS surface modification. Compared with the HCS/CS modified electrode, it is clear that the CV peak currents on N-HCSs/CS were much higher than those on HCSs/CS. The results indicated the presence of N-HCSs on the surface of bare gold electrode may provide the necessary conduction pathways

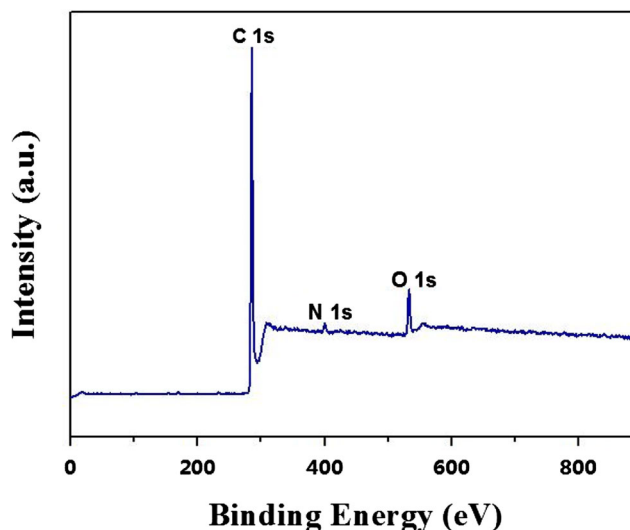


Fig. 3 **a** EDS analysis and **b** FT-IR patterns of N-HCS nanocomposite

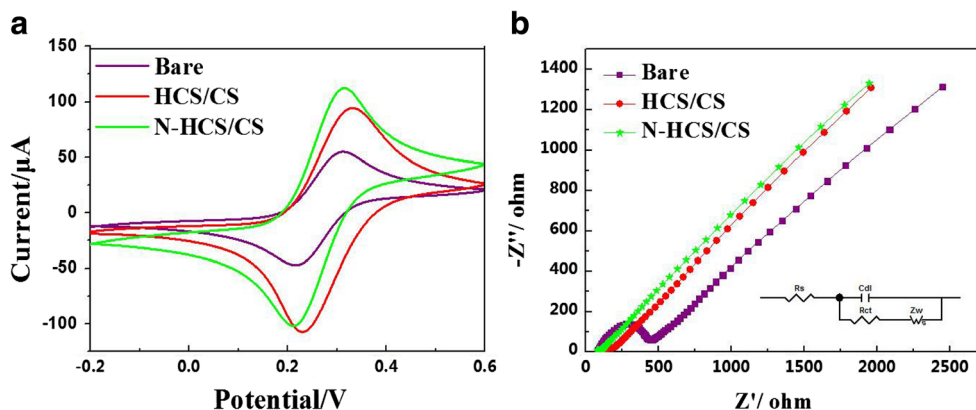
Table 1 XPS peak analysis of the N-HCS sample

| XPS peak analysis of the N-HCS sample. | | |
|--|-----------------|-----------------|
| C content (at%) | O content (at%) | N content (at%) |
| 90.32 | 6.57 | 3.11 |

on the electrode surface and a better electrochemical behavior, which could contribute to the positive charge of the chitosan and the strong adsorptive properties of N-HCSs.

In order to further characterize the electric properties of the modified electrode, Nyquist diagram of electrochemical impedance spectra (EIS) on the as-prepared modified gold electrode was employed. The equivalent circuit compatible with the Nyquist diagram recorded for different electrodes is depicted in Fig. 4b. Generally, the impedance spectrum includes a semicircle portion and a linear portion. The semicircle diameter at high frequencies corresponds to the electron transfer resistance (R_{ct}), and the linear part at lower frequencies corresponds to the diffusion process. On the bare gold electrode, the charge-transfer resistance (R_{ct}) value was got as 336.6 Ω , while on HCSs/CS, the R_{ct} value was decreased to 54.8 Ω , implying a very low electron transfer resistance of the redox probe. When modified with N-HCSs, it showed a much smaller R_{ct} ($R_{ct} \sim 20.4 \Omega$) than HCS/CS modified electrode, which implied that N-HCS was an excellent electric conducting material to accelerate the electron transfer. These results are consistent with the CV results. In comparison with HCSs, enhancement of the electrochemical activity and the conductivity is found in N-HCSs due to the doping of nitrogen. These results are consistent with previous report, nitrogen atom contains five valence electrons, and it can form strong valence bonds with carbon atoms [35, 36]. This implies that nitrogen introduced into carbon materials can break through the intrinsic chemical inertness of HCSs. Further, to improve the electrochemical performance of HCSs, we chose the N-HCSs as modifier in this work.

Fig. 4 a CV curve and b EIS plots at different electrodes in the solution of 5 mM $Fe(CN)_6^{3-/4-}$



Determination of stripping peak of Pb^{2+} , Cu^{2+} , and Hg^{2+}

In order to ensure the accuracy of stripping peak of the three HMIs, related experiments were performed. Figure 5 demonstrates that the three curves represent different SWASV stripping response of N-HCS modified electrode in 0.1 M NaAc-HAc buffer solution (pH 5.0). Clearly, the bare gold electrode (curve a) as control group has no obvious stripping peak or specific SWASV signals. Comparatively, a well-defined peak at approximately 0.48 V (curve b) is easily observed, which could be ascribed to the signal of Hg^{2+} . Then, 200 nM Pb^{2+} was added to the solution, the voltammetric peak for Hg^{2+} exhibited little growth and its signal was as well as amplified. Moreover, we also observed another stripping peak at about -0.15 V (curve c). Similarly, when 200 nM Cu^{2+} was added, we could observe its stripping peak at about 0.22 V. The positions of the other two peaks remained steady; however, their stripping current became slightly higher. This should be ascribed to the addition of the subsequent ion or enrichment of more HMIs [37]. In view of the small effect of current change, it had no impact on our experiment. Therefore, we could easily identify the position of three HMIs.

Optimization of experimental parameters

In order to obtain maximum sensitivity for detecting HMIs by using the N-HCS/CS electrode, the voltammetric parameters such as pH, deposition potential, and deposition time were optimized. Figure 6 displays the effect of different supporting electrolytes including phosphate buffer saline, NaAc-HAc, and $NH_4Cl-HCl$. Figure 6a clearly exhibits the existence of the highest oxidation peak and well-defined peak shapes when 0.1 M NaAc-HAc buffer solution was used in the experiment. The influence of the pH from 3.0 to 7.0 was then investigated. Figure 6b shows that the anodic peak currents for Pb^{2+} and Hg^{2+} gradually increase with the increase in pH from 3.0 to 5.0. Further, with the increase in pH above 5, the peak current corresponding to Pb^{2+} and Hg^{2+} decreases. Therefore, for the

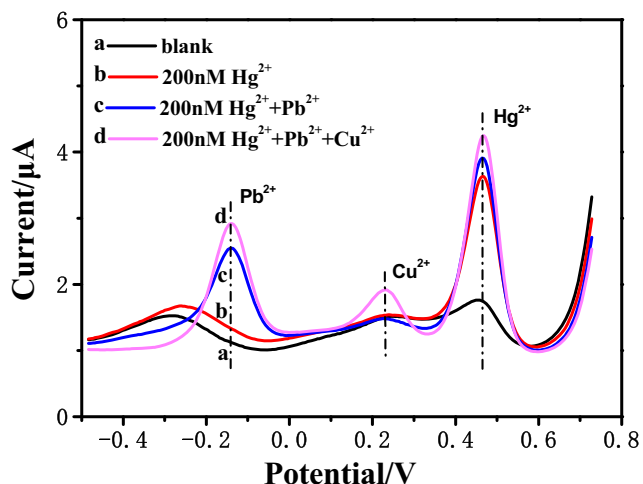


Fig. 5 SWASV responses of N-HCS/CS in the presence of Hg^{2+} , Pb^{2+} , Cu^{2+} in 0.1 M NaAc-HAc (pH = 5)

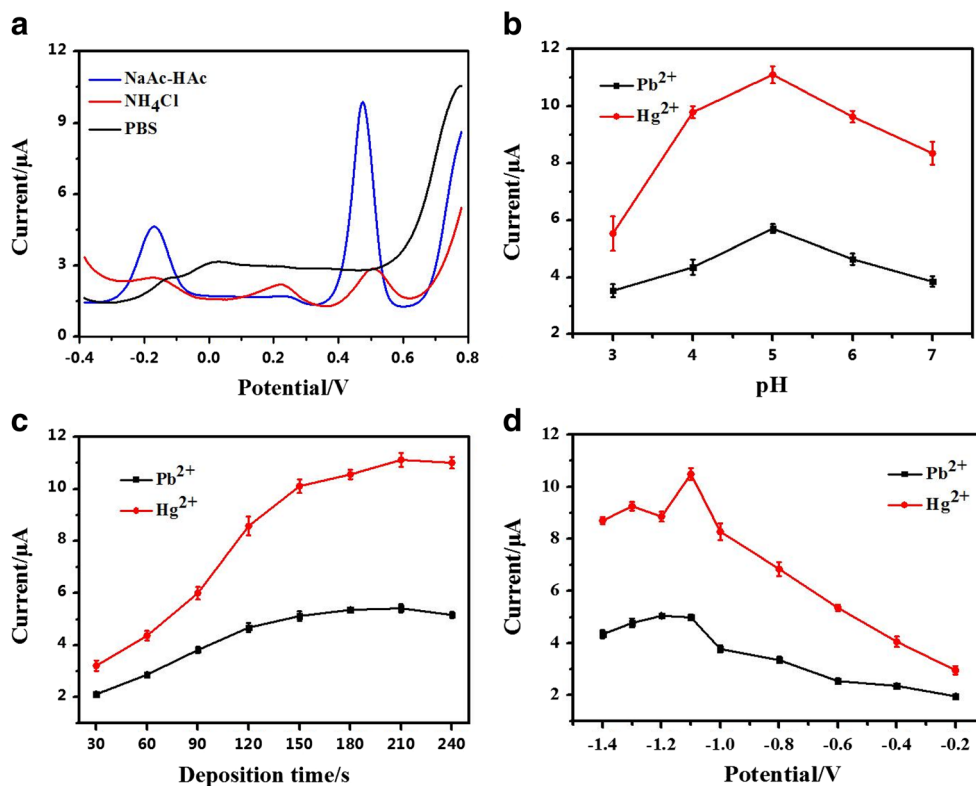
sensitivity and stability of simultaneous determination of mixed ions, pH 5 was selected as optimized value in this study. If the pH was too low, such as 3.0, the low response of N-HCS electrode toward three metal ions was probably attributed to the disruption of the N-HCSs on the electrode surface by a large number of hydrogen ions in the solution. With the increase in pH, the sensitivity was improved due to low concentration of H^+ . In contrast, if pH was too high, some stripping signals began to decrease, probably due to hydrolysis or valence change of the three types of metal ions.

Therefore, pH of 5.0 in 0.1 M NaAc-HAc buffer solution should be selected for optimization of the detection of the three HMIs by using the N-HCS electrode.

Influence of the deposition time on the detection limit and sensitivity was also investigated. Figure 6c shows the response of the stripping peak current of three target HMIs, with varying deposition time. For Pb^{2+} and Hg^{2+} , with the increase in deposition time from 30 to 150 s, the peak current increases and then almost remains stable. When the deposition time is increased to 150 s, the stripping current tends toward stability, and not much difference in the corresponding current is observed. Therefore, 150 s was selected as the optimum deposition time.

The stripping analysis indicates that the application of adequate deposition potential seems to be very important to achieve the best sensitivity. Under the above mentioned optimal conditions, the effect of deposition potential ranging from -0.2 to -1.1 V on the stripping signal of $0.5 \mu\text{M}$ Pb^{2+} after 150 s of deposition was studied. Figure 6d clearly demonstrates that when the deposition potential shifts from -1.0 to -0.2 V, a decrease in the response is observed because of the interference of the hydrogen peak. Moreover, the stripping peak current for two heavy ions reaches a maximum at -1.1 V. Thus, -1.1 V was selected as the optimal deposition potential. Notably, at a more negative potential, the hydrogen evolution affects the deposition. Thus, the deposition potential of -1.1 V was selected for the further research.

Fig. 6 Influence of **a** supporting electrolytes, **b** pH value, **c** deposition potential, and **d** deposition time on the voltammetric responses of the N-HCS/CS/ gold electrode for the simultaneous determination of Hg^{2+} and Pb^{2+}



Individual detection of various metal ions

Under the optimal experimental conditions, the differential SWASV studies were carried out for the electrochemical determination of heavy metal ions such as Hg^{2+} , Cu^{2+} , and Pb^{2+} . Hg^{2+} was determined individually at the N-HCS electrode using SWASV method. Figure 7a presented the SWASV responds toward Hg^{2+} at different concentrations. In the range of 10 to 900 nM, we could observe that linear increase in the stripping peak current was obtained with the increasing concentration of the N-HCSs. In high and low concentration ranges of 100 to 900 nM and 10 to 100 nM (inset at Fig. 7a), the linear equation were $I(\mu A) = 20.58C_{Hg(II)}(\mu M) + 0.51385$ and $I(\mu A) = 12.8C_{Hg(II)}(\mu M) + 1.36078$ (inset at Fig. 6b), with the correlation coefficient of 0.99685 and 0.99676. And the limit of detection (LOD $S/N = 3$) was calculated to be 2.35 nM. The SWASV responds of the N-HCS electrode

toward Cu^{2+} and Pb^{2+} over a concentration range from 50 to 1000 nM and 50 to 70 nM were shown in Fig. 7c, e. The linear equations for Cu^{2+} and Pb^{2+} covering the concentration range in individual determination of each ion were obtained $I(\mu A) = 5.59C_{Cu(II)}(\mu M) + 1.26488$ and $I(\mu A) = 6.32C_{Pb(II)}(\mu M) + 1.66449$, with the correlation coefficient of 0.99722 and 0.99262, respectively. From the linear equation, the detection sensitivity was $5.59 \mu A \mu M^{-1}$ for Cu^{2+} and $6.32 \mu A \mu M^{-1}$ for Pb^{2+} . In this case, the detection limits for Cu^{2+} and Pb^{2+} were 17 and 15 nM, respectively. The comparison of N-HCS/CS modified gold electrode with other modified electrodes for these metal ion determination was listed in Table 2. It could be seen that the proposed sensor was comparable and even better to the previous reports. These results indicated that N-HCS/CS modified gold electrode is an appropriate platform for the determination of these metal ions. All the results were lower than those of the specified drinking

Fig. 7 a SWASV responses with increasing Hg^{2+} concentration b the calibration plot of the linear relationship between the peak current and the concentration of Hg^{2+} , a to p, 0, 10, 20, 40, 60, 80, 100, 150, 200, 300, 400, 500, 600, 700, 800, 900 nM, respectively (inset in panel is Hg^{2+} in low concentration ranges). c SWASV responses with increasing Cu^{2+} concentration d the calibration plot of the linear relationship between the peak current and the concentration of Cu^{2+} , a to l, 0, 50, 100, 150, 200, 300, 400, 500, 600, 800, 1000 nM, respectively. e SWASV responses with increasing Pb^{2+} concentration f the calibration plot of the linear relationship between the peak current and the concentration of Pb^{2+} , a to l, 0, 50, 100, 150, 200, 250, 350, 400, 500, 600, 700 nM, respectively

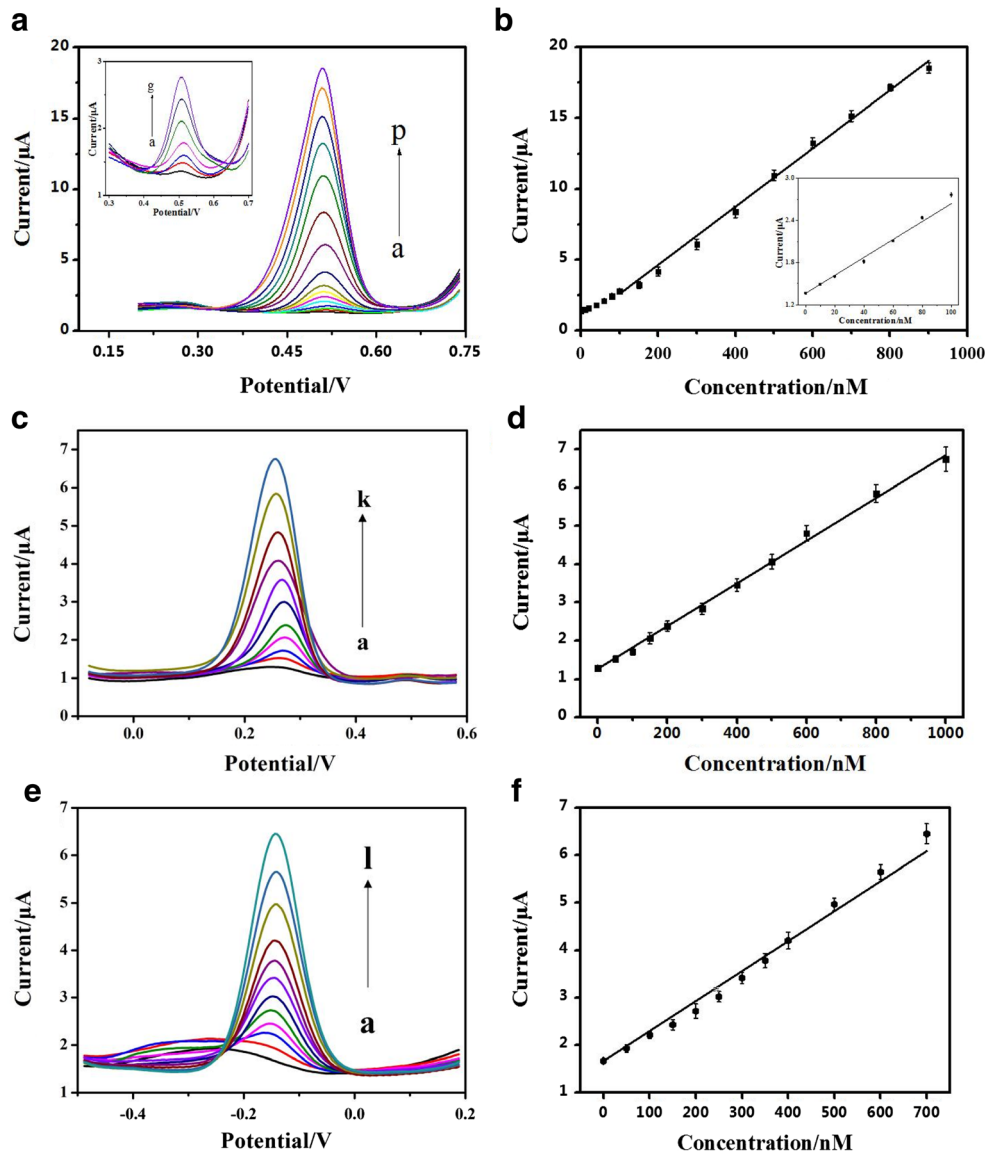


Table 2 Comparison of the proposed sensor for determination of Hg^{2+} , Cu^{2+} , and Pb^{2+} with others

| Electrode | Method | Linear ranges (μM) | Determination limits (μM) | Reference |
|-------------------------|--------|---------------------------------|--|-----------|
| L-cys-rGO/GCE | DPASV | Pb(II), 0.4–1.2 | 0.02 | [37] |
| | | Cu(II), 0.4–2 | 0.04 | |
| | | Hg(II), 0.4–2 | 0.07 | |
| Bismuth film/IL/CPE | SWASV | Pb(II), 0.48–4.8 | 0.5 | [38] |
| Schiff base/MWCNT/CPE | SWASV | Pb(II), 0.0002–0.7 | 0.6 | [39] |
| | | Hg(II), 0.0002–0.7 | 0.9 | |
| CISPE | DPSAV | Pb(II), 0.4–90 | 0.04 | [40] |
| | | Cu(II), 0.4–100 | 0.06 | |
| | | Hg(II), 0.08–50 | 0.01 | |
| N-HCS/CS/gold electrode | SWASV | Pb(II), 0.05–0.7 | 0.015 | This work |
| | | Cu(II), 0.05–1 | 0.017 | |
| | | Hg(II), 0.01–0.9 | 0.00235 | |

water standard by WHO. Overall, the N-HCS/CS modified gold electrode was proved to be an effective electrode modification material for the detection of heavy metal ions because of its excellent detection performance. We further carried out simultaneous detection of the Pb^{2+} and Hg^{2+} ions under the same optimized conditions.

Simultaneous detection of Pb^{2+} and Hg^{2+} ions

Using the optimal detection conditions described above, we further pursued the investigation of the mutual interferences between Pb^{2+} and Hg^{2+} ions at the N-HCS/CS electrode in 0.1 M NaAc-HAc buffer solution. During the procedure, the concentration of Pb^{2+} was kept constant at 0.4 μM ; however, the amount of Hg^{2+} was increased. Figure 8a displays the stripping peak current curve for Hg^{2+} in the concentration range of 50–800 nM. In this course, the stripping peak current curve of the Pb^{2+} basically remains unchanged, thus indicating that with the increase in concentration of Hg^{2+} , the stripping signal of Pb^{2+} was not affected.

Under the same condition, another experiment was performed by keeping the concentration of Hg^{2+} constant at 0.15 μM , and simply increasing the amount of Pb^{2+} . Figure 9a displays the

stripping peak current curve corresponding to Pb^{2+} with concentration in the range of 100–800 nM. With the increase in concentration of Pb^{2+} , the stripping peaks of Hg^{2+} and Pb^{2+} also increase. In this course, the concentration of the Hg^{2+} basically remains unchanged; however, its stripping peak current curve increases with the increase in the concentration of Pb^{2+} . This indicated that the increase in concentration of Pb^{2+} promoted the dissolution of Hg^{2+} . The linear equation is $I_{\text{Pb(II)}}(\mu\text{A}) = 3.97C_{\text{Pb(II)}}(\mu\text{M}) + 2.2047$ with the correlation coefficients of 0.99055. From the linear equation, the detection sensitivity was found to be $3.97 \mu\text{A} \mu\text{M}^{-1}$. And the stripping responses of Pb(II) increased by approximately 28.5%, in the presence of Hg^{2+} . The addition of Pb^{2+} enhanced the voltammetric peaks of Hg^{2+} . The current responses of 0.15 μM Hg^{2+} could reach 9 μM . Nonetheless, if the same result was required in single detection, the concentration of the Hg^{2+} must reach 0.4 μM . Combined with other literature reports, on the one hand, this result was likely due to the formation of the intermetallic compound, with the dissolution of Hg^{2+} ; thus, the current responses of Hg^{2+} enhanced but its sensitivity dropped. On the other hand, with the addition of Pb^{2+} , its concentration increased, it inclined to form a Pb film; thus, it facilitated the dissolution of Hg^{2+} [41, 42]. More importantly, in the process, because of the low

Fig. 8 a SWASV responses of the N-HCS/CS/gold electrode toward Hg^{2+} over a concentration range of 0.05 to 0.8 μM when adding 0.4 μM Pb^{2+} ; b the calibration plot of the linear relationship between the peak current and the concentration of Hg^{2+}

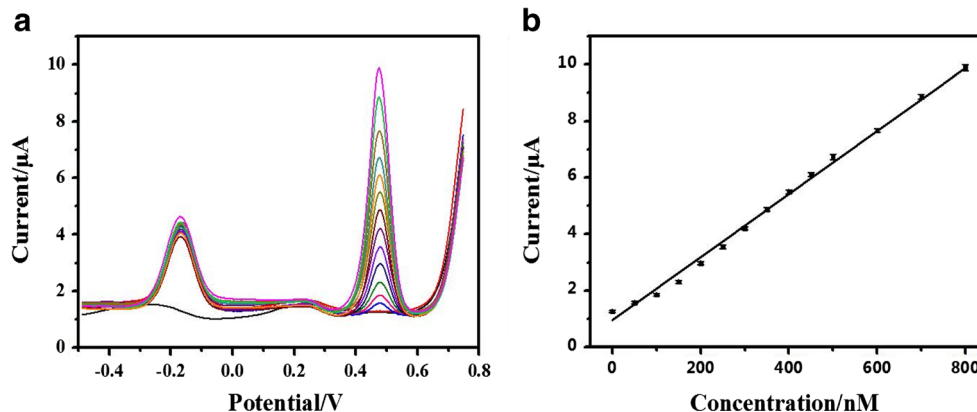
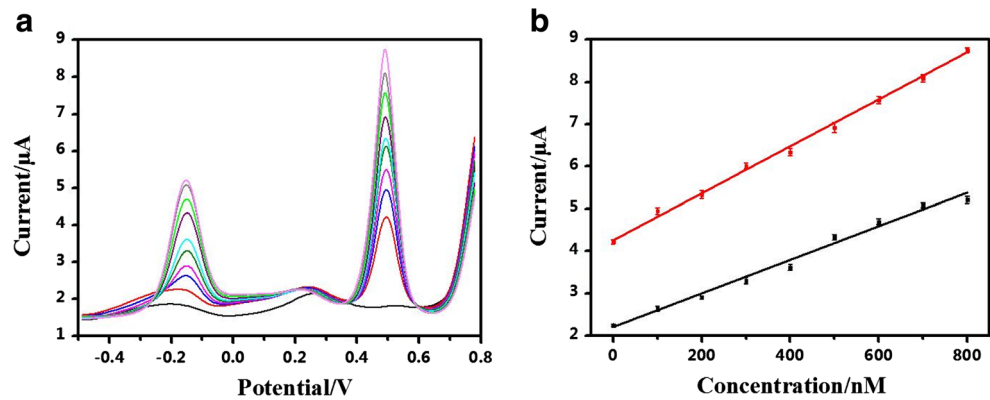


Fig. 9 **a** SWASV responses of the N-HCS/CS/gold electrode toward Pb^{2+} over a concentration range of 0.1 to 0.8 μM when adding 0.15 μM Hg^{2+} ; **b** the calibration plot of the linear relationship between the peak current and the concentration of Pb^{2+}



concentration of Hg^{2+} and low to gradually high concentration of Pb^{2+} , the ions need not compete for the active site, and the competition effect is small. Thus, it can be concluded that the proposed sensor can be successfully applied for the simultaneous determination of Pb^{2+} and Hg^{2+} .

Reproducibility, stability, and selectivity of N-HCSs/CS

N-HCS/CS modified electrode exhibited good electrochemical performance toward certain HMIs such as Pb^{2+} , Hg^{2+} , and Cu^{2+} . In order to evaluate its reproducibility and stability, SWASV method was used to detect the current response of 0.5 μM Pb^{2+} , Hg^{2+} , and Cu^{2+} in 0.1 M NaAc-HAc (pH 5.0) for seven times continuous determination. The results indicated that the stripping peak position remained the same and the stripping peak current was consistent. The relative standard deviation (RSD) was 3.6% for Pb^{2+} , 3.2% for Hg^{2+} , and 2.9% for Cu^{2+} in seven times measurements. Stability of the detection was studied under the same conditions. Furthermore, the response sensitivity retained a value of more than 95% over 2 weeks. Six electrodes were prepared from the same batch and evaluated by detecting 0.5 μM Pb^{2+} , Hg^{2+} , and Cu^{2+} . The RSD derived from the six currents for three HMIs was 3.6, 4.0, and 4.9%, respectively. The result indicated that N-HCS modified electrode exhibited excellent stability for repeated electrochemical determination of HMIs.

Conclusion

In this study, nitrogen-doped hollow carbon spheres were successfully fabricated and applied as a sensing material for individual determination of Hg^{2+} , Pb^{2+} , and Cu^{2+} , and simultaneous determination of Hg^{2+} and Pb^{2+} . During individual determination, the obtained LOD values were far below the guideline values for drinking water given by the World Health Organization. More significantly, an interesting phenomenon of mutual interference was also observed. We found that the presence of Pb^{2+} could enhance the sensitivity toward

Hg^{2+} . Thus, we expected that it was possible to use the Pb film-coated electrodes to enhance the detection sensitivity toward Hg^{2+} in further research. Thus, a reliable method toward the detection of the low concentration of Hg^{2+} was provided in this study. Excellent stability of N-HCS indicates that it can be utilized as a perfect electrode material for electrochemical detection of heavy metal ions. Furthermore, it also exhibits the promising potential for practical application for a real water sample. Finally, we demonstrated that the electrochemical sensing performance had a relationship with the adsorption capacity, which is extremely useful and important for the design of effective sensing materials.

Funding information We gratefully acknowledge the funding support of Science and Technology program of Wuhan Science and Technology Bureau (2015060202010121), the National Natural Science Foundation of China (No.21471120), International Cooperation Foundation of Hubei Province (2012IHA00201), Educational Commission of Hubei Province of China (T201306), and Scientific Research Foundation of Wuhan Institute of Technology (K201515).

References

- Vedhi C, Selvanathan G, Arumugam P, Manisankar P (2008) Electrochemical sensors of heavy metals using novel polymer-modified glassy carbon electrodes. *Ionics* 15:377
- Wang N, Sun JC, Fan H, Ai SY (2016) Anion-intercalated layered double hydroxides modified test strips for detection of heavy metal ions. *Talanta* 148:301–307. <https://doi.org/10.1016/j.talanta.2015.11.007>
- Ma HC, An R, Chen LL, YH F, Ma C, Dong XL, Zhang XF (2015) A study of the photodeposition over Ti/TiO₂ electrode for electrochemical detection of heavy metal ions. *Electrochem Commun* 57: 18–21. <https://doi.org/10.1016/j.elecom.2015.04.015>
- Ji WB, Yap SHK, Panwar N, Zhang LL, Lin B, Yong KT, Tjin SC (2016) Detection of low-concentration heavy metal ions using optical microfiber sensor. *Sensors Actuat B Chem* 237:142–149. <https://doi.org/10.1016/j.snb.2016.06.053>
- Wang N, Lin M, Dai H, Ma H (2016) Functionalized gold nanoparticles/reduced graphene oxide nanocomposites for ultrasensitive electrochemical sensing of mercury ions based on thymine-mercury-thymine structure. *Biosens Bioelectron* 79:320–326. <https://doi.org/10.1016/j.bios.2015.12.056>
- Afkhami A, Madrakian T, Sabounchei SJ, Rezaei M, Samiee S, Poursahbaz M (2012) Construction of a modified carbon paste

- electrode for the highly selective simultaneous electrochemical determination of trace amounts of mercury(II) and cadmium(II). *Sensors Actuat B Chem* 161(1):542–548. <https://doi.org/10.1016/j.snb.2011.10.073>
7. Dedelaite L, Kizilkaya S, Incebay H, Ramanavicius A (2015) Electrochemical determination of Cu(II) ions using glassy carbon electrode modified by some nanomaterials and 3-nitroaniline. *Colloid Surface A* 483:279–284. <https://doi.org/10.1016/j.colsurfa.2015.05.054>
 8. Xiao C, Chu XC, Yang Y, Li X, Zhang XH, Chen JH (2011) Hollow nitrogen-doped carbon microspheres pyrolyzed from self-polymerized dopamine and its application in simultaneous electrochemical determination of uric acid, ascorbic acid and dopamine. *Biosens Bioelectron* 26(6):2934–2939. <https://doi.org/10.1016/j.bios.2010.11.041>
 9. Zhou L, Xiong W, Liu ST (2015) Size-controlled growth of gold nanoparticle-doped carbon foams as sensitive electrochemical sensors for the determination of Pb(II). *Ionics* 22:935
 10. Bagheri H, Afkhami A, Khoshsafar H, Rezaei M, Shirzadmehr A (2013) Simultaneous electrochemical determination of heavy metal using a triphenylphosphine/MWCNTs composite carbon ionic liquid electrode. *Sensors Actuat B Chem* 186:451–460. <https://doi.org/10.1016/j.snb.2013.06.051>
 11. Zhu L, LL X, Huang BZ, Jia NM, Tan L, Yao SZ (2014) Simultaneous determination of Cd(II) and Pb(II) using square wave anodic stripping voltammetry at a gold nanoparticle-graphene-cysteine composite modified bismuth film electrode. *Electrochim Acta* 115:471–477. <https://doi.org/10.1016/j.electacta.2013.10.209>
 12. Zhang YX, Zhang JM, Liu Y, Huang H, Kang ZH (2012) Highly ordered three-dimensional macroporous carbon spheres for determination of heavy metal ions. *Mater Res Bull* 47(4):1034–1039. <https://doi.org/10.1016/j.materresbull.2011.12.051>
 13. Li XY, Zhou HH, Fu CP, Wang F, Ding YJ, Kuang YF (2016) A novel design of engineered multi-walled carbon nanotubes material and its improved performance in simultaneous detection of Cd(II) and Pb(II) by square wave anodic stripping voltammetry. *Sensors Actuat B Chem* 236:144–152. <https://doi.org/10.1016/j.snb.2016.05.149>
 14. Enterría M, Figueiredo JL (2016) Nanostructured mesoporous carbons: tuning texture and surface chemistry. *Carbon* 108:79–102. <https://doi.org/10.1016/j.carbon.2016.06.108>
 15. Chen XY, Chen C, Zhang ZJ, Xie DH, Deng X, Liu JW (2013) Nitrogen-doped porous carbon for supercapacitor with long-term electrochemical stability. *J Power Sources* 230:50–58. <https://doi.org/10.1016/j.jpowsour.2012.12.054>
 16. Dai YH, Jiang H, YJ H, Fu Y, Li CZ (2014) Controlled synthesis of ultrathin hollow mesoporous carbon nanospheres for supercapacitor applications. *Ind Eng Chem Res* 53(8):3125–3130. <https://doi.org/10.1021/ie403950t>
 17. White RJ, Tauer K, Antonietti M, Titirici MM (2010) Functional hollow carbon nanospheres by latex templating. *J Am Chem Soc* 132:17360
 18. Nongwe I, Ravat V, Meijboom R, Coville NJ (2013) Efficient and reusable Co/nitrogen doped hollow carbon sphere catalysts for the aerobic oxidation of styrene. *Appl Catal A Gen* 466:1–8. <https://doi.org/10.1016/j.apcata.2013.06.014>
 19. Yi YH, Zhu GB, Sun H, Sun JF, Wu XY (2016) Nitrogen-doped hollow carbon spheres wrapped with graphene nanostructure for highly sensitive electrochemical sensing of parachlorophenol. *Biosens Bioelectron* 86:62–67. <https://doi.org/10.1016/j.bios.2016.06.034>
 20. Zhang WM, JS H, Guo YG, Zheng SF, Zhong LS (2008) Tin-nanoparticles encapsulated in elastic hollow carbon spheres for high-performance anode material in lithium-ion batteries. *Adv Mater* 20(6):1160–1165. <https://doi.org/10.1002/adma.200701364>
 21. Sun H, Zhu YQ, Yang B, Wang YF, Wu YP, Du JZ (2016) Template-free fabrication of nitrogen-doped hollow carbon spheres for high-performance supercapacitors based on a scalable homopolymer vesicle. *J Mater Chem A* 4(31):12088–12097. <https://doi.org/10.1039/C6TA04330E>
 22. Chen L, Ji T, LW M, Zhu JH (2017) Carbon cotton fabric derived hierarchically porous carbon and nitrogen doping for sustainable capacitor electrode. *Carbon* 111:839–848. <https://doi.org/10.1016/j.carbon.2016.10.054>
 23. Zhan YF, Yu X, Cao LM, Zhang BD, Wu XX, Xie WG, Mai WJ, Meng H (2016) The influence of nitrogen source and doping sequence on the electrocatalytic activity for oxygen reduction reaction of nitrogen doped carbon materials. *Int J Hydrogen Energ* 41:3493
 24. Sun F, Gao JH, Pi XX, Wang LJ, Yang YQ, ZB Q, Wu SH (2017) High performance aqueous supercapacitor based on highly nitrogen-doped carbon nanospheres with unimodal mesoporosity. *J Power Sources* 337:189–196. <https://doi.org/10.1016/j.jpowsour.2016.10.086>
 25. Sun F, Gao JH, Liu X, Yang YQ, SH W (2016) Controllable nitrogen introduction into porous carbon with porosity retaining for investigating nitrogen doping effect on SO₂ adsorption. *Chem Eng J* 290:116–124. <https://doi.org/10.1016/j.cej.2015.12.044>
 26. Chen AB, Li YQ, Liu L, YF Y, Xia KC, Wang YY (2017) Controllable synthesis of nitrogen-doped hollow mesoporous carbon spheres using ionic liquids as template for supercapacitors. *Appl Surf Sci* 393:151–158. <https://doi.org/10.1016/j.apsusc.2016.10.025>
 27. Zhou TS, Zhou Y, Ma RG, Zhou ZZ, Liu GH, Liu Q, Zhu YF, Wang JC (2016) In situ formation of nitrogen-doped carbon nanoparticles on hollow carbon spheres as efficient oxygen reduction electrocatalysts. *Nano* 8:18134
 28. Huang JS, Zhang XP, Zhou LM, You TY (2016) Simultaneous electrochemical determination of dihydroxybenzene isomers using electrospun nitrogen-doped carbon nanofiber film electrode. *Sensors Actuat B Chem* 224:568–576. <https://doi.org/10.1016/j.snb.2015.10.102>
 29. Chen AB, YF Y, Lv HJ, Wang YY, Shen SF, YQ H, Li B, Zhang Y, Zhang J (2013) Thin-walled, mesoporous and nitrogen-doped hollow carbon spheres using ionic liquids as precursors. *J Mater Chem A* 1(4):1045–1047. <https://doi.org/10.1039/C2TA01013E>
 30. Zhang ZH, Zhang R, Li CC, Yuan L, Li PP, Yao L, Liu SQ (2012) Nitrogen-doped carbon hollow spheres for immobilization, direct electrochemistry, and biosensing of protein. *Electroanalysis* 24(6):1424–1430. <https://doi.org/10.1002/elan.201200002>
 31. Zeng MF, Wang YD, Liu Q, Yuan X, Feng RK, Yang Z, Qi CZ (2016) N-doped mesoporous carbons supported palladium catalysts prepared from chitosan/silica/palladium gel beads. *Int J Biol Macromol* 89:449–455. <https://doi.org/10.1016/j.ijbiomac.2016.05.011>
 32. Wen YF, Wang B, Luo B, Wang LZ (2016) Long-term cycling performance of nitrogen-doped hollow carbon nanospheres as anode materials for sodium-ion batteries. *Eur J Inorg Chem* 2016(13–14):2051–2055. <https://doi.org/10.1002/ejic.201501172>
 33. Xiong W, Zhou L, Liu S (2016) A new electrochemical sensor based on carboimidazole grafted reduce graphene oxide for simultaneous detection of Hg²⁺ and Pb²⁺. *Chem Eng J* 284:650–656. <https://doi.org/10.1016/j.cej.2015.09.013>
 34. Sun GL, Ma LY, Ran JB, Li B, Shen XY, Tong H (2016) Templated synthesis and activation of highly nitrogen-doped worm-like carbon composites based on melamine-urea-formaldehyde resins for high performance supercapacitors. *Electrochim Acta* 194:168–178. <https://doi.org/10.1016/j.electacta.2016.02.066>
 35. Soares OSGP, Rocha RP, Gonçalves AG, Figueiredo JL, Órfão JJM, Pereira MFR (2016) Highly active N-doped carbon nanotubes prepared by an easy ball milling method for advanced oxidation

- processes. *Appl Catal B Environ* 192:296–303. <https://doi.org/10.1016/j.apcatb.2016.03.069>
36. Galeano C, Meier JC, Soorholtz M, Bongard H, Baldizzone C, Mayrhofer KJJ (2014) Nitrogen-doped hollow carbon spheres as a support for platinum-based electrocatalysts. *ACS Catal* 4(11):3856–3868. <https://doi.org/10.1021/cs5003492>
 37. Muralikrishna S, Sureshkumar K, Varley TS, Nagaraju DH, Ramakrishnappa T (2014) In situ reduction and functionalization of graphene oxide with L-cysteine for simultaneous electrochemical determination of cadmium(II), lead(II), copper(II), and mercury(II) ions. *Anal Methods* 6(21):8698–8705. <https://doi.org/10.1039/C4AY01945H>
 38. Ping JF, Wu J, Ying YB, Wang MH, Liu G, Zhang M (2011) Evaluation of trace heavy metal levels in soil samples using an ionic liquid modified carbon paste electrode. *J Agr Food Chem* 59(9):4418–4423. <https://doi.org/10.1021/jf200288e>
 39. Afkhami A, Bagheri H, Khoshsafar H, Saber-Tehrani M, Tabatabaee M, Shirzadmehr A (2012) Simultaneous trace-levels determination of Hg(II) and Pb(II) ions in various samples using a modified carbon paste electrode based on multi-walled carbon nanotubes and a new synthesized Schiff base. *Anal Chim Acta* 746:98–106. <https://doi.org/10.1016/j.aca.2012.08.024>
 40. Xing HK, Xu JK, Zhu XF, Duan XM, Lu LM, Wang WM, Zhang YS, Yang TT (2016) Highly sensitive simultaneous determination of cadmium (II), lead (II), copper (II), and mercury (II) ions on N-doped graphene modified electrode. *J Electroanal Chem* 760:52–58. <https://doi.org/10.1016/j.jelechem.2015.11.043>
 41. Guan Q, Xiong W, Zhou L, Liu ST (2016) Facile synthesis of nitrogen-doped porous carbon-gold hybrid nanocomposite for mercury(II) ion electrochemical determination. *Electroanalysis* 28(1):133–139. <https://doi.org/10.1002/elan.201500481>
 42. Xing HK, Xu JK, Zhu XF, Duan XM, Lu LM, Zuo YX, Zhang YS, Wang WM (2016) A new electrochemical sensor based on carboimidazole grafted reduced graphene oxide for simultaneous detection of Hg²⁺ and Pb²⁺. *J Electroanal Chem* 782:250–255. <https://doi.org/10.1016/j.jelechem.2016.10.043>